Nuclear Instruments and Methods in Physics Research A 659 (2011) 428–433

Contents lists available at SciVerse ScienceDirect

Nuclear Instruments and Methods in Physics Research A

journal homepage: www.elsevier.com/locate/nima

Early warning for VHE gamma-ray flares with the ARGO-YBJ detector

B. Bartoli [a,b], P. Bernardini [c,d], X.J. Bi [e], C. Bleve [c,d], I. Bolognino [f,g], P. Branchini [h], A. Budano [h], A.K. Calabrese Melcarne [i], P. Camarri [j,k], Z. Cao [e], A. Cappa [l,m], R. Cardarelli [k], S. Catalanotti [a,b], C. Cattaneo [g], P. Celio [h,n], S.Z. Chen [e], T.L. Chen [o], Y. Chen [e,*], P. Creti [d], S.W. Cui [p], B.Z. Dai [q], G. D'Alí Staiti [r,s], Danzengluobu [o], M. Dattoli [l,m,t], I. De Mitri [c,d], B. D'Ettorre Piazzoli [a,b], T. Di Girolamo [a,b], X.H. Ding [o], G. Di Sciascio [k], C.F. Feng [u], Zhaoyang Feng [e], Zhenyong Feng [v], F. Galeazzi [h], P. Galeotti [m,t], E. Giroletti [f,g], Q.B. Gou [e], Y.Q. Guo [e], H.H. He [e], Haibing Hu [o], Hongbo Hu [e], Q. Huang [v], M. Iacovacci [a,b], R. Iuppa [j,k], I. James [h,n], H.Y. Jia [v], Labaciren [o], H.J. Li [o], J.Y. Li [u], X.X. Li [e], G. Liguori [f,g], C. Liu [e], C.Q. Liu [q], J. Liu [q], M.Y. Liu [o], H. Lu [e], X.H. Ma [e], G. Mancarella [c,d], S.M. Mari [h,n], G. Marsella [d,w], D. Martello [c,d], S. Mastroianni [b], P. Montini [h,n], C.C. Ning [o], A. Pagliaro [s,x], M. Panareo [d,w], B. Panico [j,k], L. Perrone [d,w], P. Pistilli [h,n], X.B. Qu [u], E. Rossi [b], F. Ruggieri [h], P. Salvini [g], R. Santonico [j,k], P.R. Shen [e], X.D. Sheng [e], F. Shi [e], C. Stanescu [h], A. Surdo [d], Y.H. Tan [e], P. Vallania [l,m], S. Vernetto [m], C. Vigorito [m,t], B. Wang [e], H. Wang [e], C.Y. Wu [e], H.R. Wu [e], B. Xu [v], L. Xue [u], Y.X. Yan [q], Q.Y. Yang [q], X.C. Yang [q], Z.G. Yao [e], A.F. Yuan [o], M. Zha [e], H.M. Zhang [e], Jilong Zhang [e], Jianli Zhang [e], L. Zhang [q], P. Zhang [q], X.Y. Zhang [u], Y. Zhang [e], Zhaxiciren [o], Zhaxisangzhu [o], X.X. Zhou [v], F.R. Zhu [v], Q.Q. Zhu [e], G. Zizzi [i]

[a] *Dipartimento di Fisica dell'Università di Napoli "Federico II", Complesso Universitario di Monte Sant'Angelo, via Cinthia, 80126 Napoli, Italy*
[b] *Istituto Nazionale di Fisica Nucleare, Sezione di Napoli, Complesso Universitario di Monte Sant'Angelo, via Cinthia, 80126 Napoli, Italy*
[c] *Dipartimento di Fisica dell'Università del Salento, via per Arnesano, 73100 Lecce, Italy*
[d] *Istituto Nazionale di Fisica Nucleare, Sezione di Lecce, via per Arnesano, 73100 Lecce, Italy*
[e] *Key Laboratory of Particle Astrophysics, Institute of High Energy Physics, Chinese Academy of Sciences, P.O. Box 918, 100049 Beijing, PR China*
[f] *Dipartimento di Fisica Nucleare e Teorica dell'Università di Pavia, via Bassi 6, 27100 Pavia, Italy*
[g] *Istituto Nazionale di Fisica Nucleare, Sezione di Pavia, via Bassi 6, 27100 Pavia, Italy*
[h] *Istituto Nazionale di Fisica Nucleare, Sezione di Roma Tre, via della Vasca Navale 84, 00146 Roma, Italy*
[i] *Istituto Nazionale di Fisica Nucleare – CNAF, Viale Berti-Pichat 6/2, 40127 Bologna, Italy*
[j] *Dipartimento di Fisica dell'Università di Roma "Tor Vergata", via della Ricerca Scientifica 1, 00133 Roma, Italy*
[k] *Istituto Nazionale di Fisica Nucleare, Sezione di Roma Tor Vergata, via della Ricerca Scientifica 1, 00133 Roma, Italy*
[l] *Istituto di Fisica dello Spazio Interplanetario dell'Istituto Nazionale di Astrofisica, corso Fiume 4, 10133 Torino, Italy*
[m] *Istituto Nazionale di Fisica Nucleare, Sezione di Torino, via P. Giuria 1, 10125 Torino, Italy*
[n] *Dipartimento di Fisica dell'Università "Roma Tre", via della Vasca Navale 84, 00146 Roma, Italy*
[o] *Tibet University, 850000 Lhasa, Xizang, PR China*
[p] *Hebei Normal University, Shijiazhuang 050016, Hebei, PR China*
[q] *Yunnan University, 2 North Cuihu Rd, 650091 Kunming, Yunnan, PR China*
[r] *Università degli Studi di Palermo, Dipartimento di Fisica e Tecnologie Relative, Viale delle Scienze, Edificio 18, 90128 Palermo, Italy*
[s] *Istituto Nazionale di Fisica Nucleare, Sezione di Catania, Viale A. Doria 6, 95125 Catania, Italy*
[t] *Dipartimento di Fisica Generale dell'Università di Torino, via P. Giuria 1, 10125 Torino, Italy*
[u] *Shandong University, 250100 Jinan, Shandong, PR China*
[v] *Southwest Jiaotong University, 610031 Chengdu, Sichuan, PR China*
[w] *Dipartimento di Ingegneria dell'Innovazione, Università del Salento, 73100 Lecce, Italy*
[x] *Istituto di Astrofisica Spaziale e Fisica Cosmica, Istituto Nazionale di Astrofisica, via La Malfa 153, 90146 Palermo, Italy*

The ARGO-YBJ Collaboration

* Corresponding author. Tel.: +86 10 88236106; fax: +86 10 88233086.
E-mail address: yao.chen@ihep.ac.cn (Y. Chen).

0168-9002/$ - see front matter
doi:10.1016/j.nima.2011.09.013

ARTICLE INFO

Article history:
Received 9 May 2011
Received in revised form
21 July 2011
Accepted 5 September 2011
Available online 17 September 2011

Keywords:
Monitoring
Flaring phenomenon
VHE extragalactic source
Wide field of view
ARGO-YBJ

ABSTRACT

Detecting and monitoring emissions from flaring gamma-ray sources in the very-high-energy (VHE, > 100 GeV) band is a very important topic in gamma-ray astronomy. The ARGO-YBJ detector is characterized by a high duty cycle and a wide field of view. Therefore, it is particularly capable of detecting flares from extragalactic objects. Based on fast reconstruction and analysis, real-time monitoring of 33 selected VHE extragalactic sources is implemented. Flares exceeding a specific threshold are reported timely, hence enabling the follow-up observation of these objects using more sensitive detectors, such as Cherenkov telescopes.

1. Introduction

At present, more than 40 extragalactic sources have been detected by Imaging Atmospheric Cherenkov Telescopes (IACTs) to have an energy above 100 GeV [1,2]. Most of these sources, around 30, belong to the blazar class of active galactic nuclei (AGNs), mainly as BL Lac objects. The emission from blazars is highly variable and is characterized by a flaring behavior, in which the flux increases dramatically on various time scales, even down to the hour time scale. Many interesting studies in physics can be done on the flaring phenomenon or variability studies. For instance, spectral variations of gamma rays from the sources are used as a tool to understand the physics of the source. Therefore, studying or monitoring their variability with sufficiently low exposure times is necessary.

A high duty cycle ($\sim$95%) and a wide aperture ($\sim$2 sr) of ARGO-YBJ allow the detection of flaring behavior associated with these AGNs, if whose flare emissions are intense enough. Two very interesting flaring events have been observed by ARGO-YBJ. First, in June 2008 [3], ARGO-YBJ successfully observed flares of Mrk 421 on a timescale of 3 days, whereas IACTs could not do so due to moonlight. In February 2010, an excess signal (around 4 standard deviation (s.d.)) from Mrk 421 is captured within a one-day transit [4]. These observations confirm that ARGO-YBJ is capable of the real-time monitoring of transient phenomena associated with variable sources.

The present study conducts real-time monitoring of selected extragalactic flaring sources. Section 2 briefly describes the experiment setup and Section 3 introduces the candidate sources. The details of the monitoring procedure are described in Section 4: time calibration, event selection, and fast reconstruction. This is followed by the presentation of the background estimation and the search for an excess in the nearby cells and in the running windows. Then the alarm threshold and chance probability are described. The results of the test run are presented in Section 5.

2. ARGO-YBJ experiment

The ARGO-YBJ detector is located at the Yang-Ba-Jing Cosmic Ray Observatory (Tibet, China, 30.11° N, 90.53° E) at an altitude of 4300 m a.s.l., corresponding to a vertical atmospheric depth of 606 g/cm^2. It consists of a single layer of Resistive Place Chambers (RPCs), with each RPC (2.8×1.25 m^2) divided into 10 basic detection units called pads (55.6×61.8 cm^2). Each pad consists of eight digital readout strips. Twelve RPCs are grouped into a cluster (5.7×7.6 m^2). The central carpet (78×74 m^2) of the detector is fully covered by 130 clusters, whereas 23 clusters form a guard ring surrounding the central carpet for a better shower core reconstruction. The whole array covers a total area of about 11,000 m^2. To extend the dynamic range, a charge read-out layer has been implemented by instrumenting each RPC with two large-size pads called "big-pad" (140×122.5 cm^2 each) [5].

Two independent DAQ systems are implemented in the detector: the scaler mode and the shower mode. In the current work,

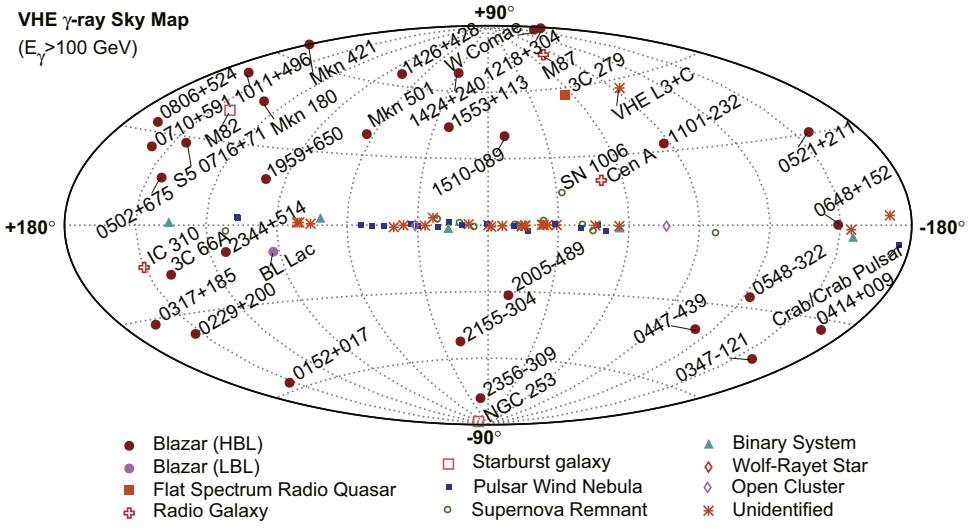

Fig. 1. The sky map showing all selected sources. Adopted from [1], updated on 2010/03/31 only.

Table 1
List of selected candidates. The parameters of these sources, such as flux, spectrum and redshift, are obtained from the reference papers provided in [1]; and another two: [8] for Crab, [7] for VHE L3+C.

Name	RA (degree)	DEC (degree)	E_{th} (GeV)	Flux ($>E_{th}$) (crab)	Index	Redshift
Mrk 421	166.114	38.209	500	3.00×10^{-1}	−2.00	0.030
Mrk 501	253.468	39.760	300	6.60×10^{-2}	−2.20	0.034
1ES 2344+514	356.653	51.708	350	6.90×10^{-1}	−2.15	0.044
1ES 1959+650	299.995	65.151	600	2.00×10^{0}	N/A	0.047
1H 1426+428	217.136	42.672	280	1.40×10^{-1}	−3.55	0.129
M87	187.706	12.391	880	4.00×10^{-2}	N/A	0.0044
1ES 1218+304	185.341	30.177	250	4.80×10^{-1}	−3.00	0.182
1ES 1101-232	165.907	−23.492	160	2.20×10^{-2}	−2.88	0.186
PG 1553+113	238.929	11.190	200	2.00×10^{-2}	−4.00	>0.09
Mrk 180	174.110	70.158	200	2.50×10^{-2}	−3.60	0.045
BL Lacertae	330.680	42.278	200	2.50×10^{-2}	−3.60	0.069
1ES 0229+200	38.203	20.288	580	2.20×10^{-2}	−2.50	0.140
1ES 0347-121	57.347	−11.991	250	2.00×10^{-2}	−3.10	0.185
1ES 1011+496	153.767	49.434	200	6.70×10^{-2}	−4.00	0.212
3C 279	194.047	−5.789	100	7.07×10^{-1}	−4.10	0.536
RGB J0152+017	28.165	1.788	300	2.20×10^{-2}	−2.95	0.080
1ES 0806+524	122.455	52.316	300	1.80×10^{-2}	−3.60	0.138
W Comae	185.382	28.233	200	8.40×10^{-2}	−3.81	0.102
S5 0716+71	110.473	71.343	400	1.30×10^{-1}	N/A	0.31
3C 66A	35.665	43.036	200	5.50×10^{-2}	−4.10	0.444
RGB J0710+591	107.625	59.139	300	1.60×10^{-2}	N/A	0.125
PKS 1424+240	216.752	23.800	200	2.00×10^{-2}	N/A	N/A
NGC 253	11.890	−25.288	220	3.00×10^{-3}	−2.20	0.0008
M82	148.843	69.661	700	1.20×10^{-2}	−2.60	0.0007
VER J0521+211	80.480	21.190	200	5.00×10^{-2}	N/A	N/A
RBS 0413	49.966	18.759	200	2.00×10^{-2}	N/A	0.19
1ES 0414+009	64.218	1.090	200	5.00×10^{-3}	N/A	0.287
1ES 0502+675	76.985	67.650	350	4.00×10^{-2}	N/A	0.341
PKS 1510-089	228.210	−8.900	N/A	N/A	N/A	0.36
RGB 0648+152	102.207	15.273	200	2.00×10^{-2}	N/A	N/A
IC 310	49.179	41.325	300	2.50×10^{-2}	N/A	0.019
VHE L3+C	172.530	−1.190	36	4.86×10^{5}	−6.31	N/A
Crab	83.633	22.014	200	1.00×10^{0}	−2.62	0

only the data from the shower mode are used. In this mode, the arrival time and fired strip pattern of each fired pad are recorded for subsequent geometric reconstruction. The trigger threshold refers to the number of fired pads greater than 20 within the 420 ns triggering window, whereas the trigger rate is about 3.5 kHz [6]. The completed ARGO-YBJ detector has been collecting data since November 2007.

3. Source selection

A list of VHE extragalactic candidates collected by Wagner [1] (Fig. 1) are chosen for the monitoring procedure. From this list, only 31 sources are within the field of view of the ARGO-YBJ detector. VHE L3+C [7] is added to the list upon the authors' curiosity, and the Crab Nebula is added to supervise frequently the monitoring procedure and ensure that it is stable. Moreover, it also acts as a direct indication of the sensitivity of the detector to a steady VHE point source. Table 1 shows all the 33 candidates.

4. Monitoring scheme

4.1. Calibration and event selection

An off-line time calibration procedure [9] is adopted to remove systematic time effects from the read-out channels. In this fast-reconstruction mode, the time calibration data for the last period are used instead of those of the current period, which will be officially produced every 10 days based on data. Fig. 2 shows the distributions of the opening angle using different time calibrations for the same sets of data. We found that the difference is less than 0.1°. Therefore, only trivial effects are produced while taking into account an angular resolution of the detector at about 0.8° for a pad multiplicity greater than 100—obtained from a full Monte Carlo simulation.

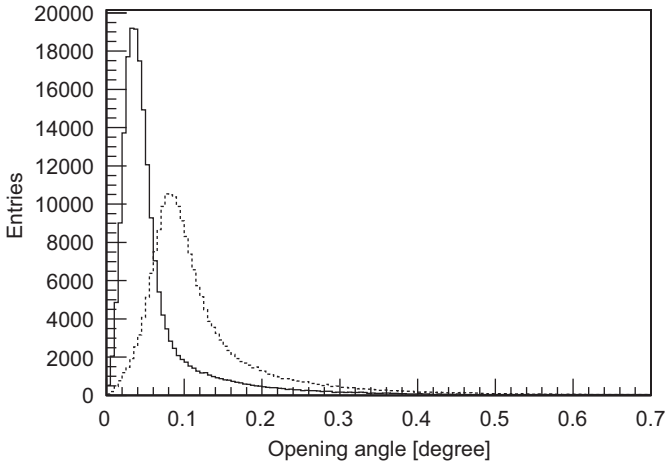

Fig. 2. Distribution of the space angle between two directions of an event reconstructed based on two different time calibration data. The solid line represents two consecutive time calibration data, whereas the dashed line stands for two time calibration data separated by 30 days.

A single run of the ARGO-YBJ detector usually lasts for a couple of hours. Raw data are split into tens of files, each with a duration of about 7 min. A raw data file is transferred to the IHEP (Institute of High Energy Physics, Beijing) and INFN (Istitute Nazionale di Fisica, Roma) computer center through the Internet usually within half an hour after its creation. After receiving a raw data

file, the reconstruction program starts to process it automatically. Raw data reconstruction is the most time-consuming process in the whole analysis procedure. Considering the detector's high trigger rate and the limited angular resolution at low energy, only events with the number of fired pads greater than 100 can be used, thus the median value of the energy distribution is 1.8 TeV, assuming a spectral index of 2.4. The data set used in this analysis contained all showers with a zenith angle less than 60°. No other event selections are applied. On a typical CPU, a file can be reconstructed within 2 h. For this study, we employed an average of 15 CPUs.

4.2. Search for excess

4.2.1. Background estimate

The surrounding region method [7] is used for estimating the background. Briefly, this method relies on the fact that the ratio, $1/R$, of events from a region located around the cell of interest to the number of events of the signal region remains constant for a fixed direction with respect to the detector. It can be measured by the experiment over a long period. By measuring the number of events in the signal region within the same time interval and by knowing R, the expected number of background events in the cell of interest can be calculated. Then the Li-Ma prescription [10] is adopted to calculate the significance. To match angular resolution and the significance optimization, the sky-cell bin widths are set equal to $\Delta\delta = 1.8^\circ$ in declination and $\Delta\alpha \simeq \Delta\delta/\cos\delta$ in right ascension. The half-widths of the background region are from $w_a = 0.75 \times \Delta\delta$ to $w_b = \Delta\delta + 2^\circ$ in declination and from $w_a \times (\Delta\alpha/\Delta\delta)$ to $w_b \times (\Delta\alpha/\Delta\delta)$ in right ascension.

Fig. 3 shows the significance distribution of all sky cells for data collected within one day, which are arbitrarily selected in 2010. Data are well-fitted to a normal distribution, indicating that the method employed produced excellent background estimation.

4.2.2. Sky cell shifts

Several issues should be considered when choosing the sky cells for a source:

(a) The source should not reside exactly at the center of a sky cell because sky cell divisions are defined beforehand without optimization to any source;
(b) Precise correction to the systematic pointing error of ARGO-YBJ is not applied in the current study because of its dependence on event selection criteria and source positions. From moon-shadow analysis [11], with a significance of 55 s.d., a systematic shift of the moon shadow of $(0.19 \pm 0.02)^\circ$ toward the north is observed.

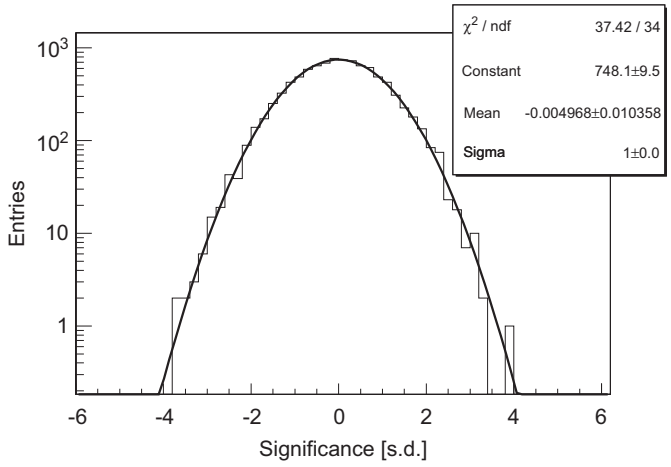

Fig. 3. Significance distribution of all sky cells for 1 day's data.

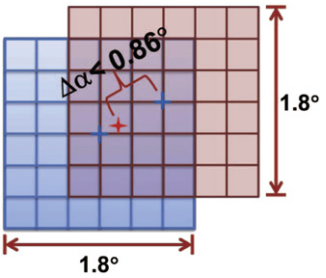

Fig. 4. Schematic plot about the shifting of sky cells to determine maximal significance.

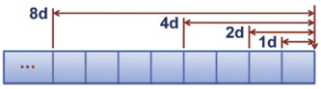

Fig. 5. Schematic plot about the overlapped time binnings.

To avoid the positioning problems shown in Fig. 4, 36 shifts are employed on every sky cell, with a space of 1/6 cell width both in declination and in right ascension. Among these shifts, only the 24 nearest sky cells (equivalently, removing the three shifts in each of the four corners) are adopted for every source, in order to restrict a reasonable angular distance between the cell center and the source. The maximum distance between the center of any of these adopted sky cells and the source position is less than 0.86°. The shifted 24 sky cells overlap each other and their events are correlated. For a specific source, only the maximum significant excess among these nearby cells is kept, indicating the significance of the source.

4.2.3. Duration search

At present, no well-accepted theoretical model has been developed to understand the duration of the transient flaring phenomenon. Observation of Mrk 421 indicates that a flare may last from several hours to several days.

In the analysis, each source is monitored until it disappeared from the field of view of the detector (zenith angle $> 60^\circ$). Upon its disappearance, the excess significance of 1, 2, 4, and 8 day transits (i.e., sidereal days) are calculated immediately, and the maximum is taken to represent the significance of the source for that day (Fig. 5).

Thus, a sidereal daily maximum significance of a given source is identified from 24 cell shifts and four time binnings.

4.3. Alarm

As previously discussed, the excess of any source is searched from 24 sky cells nearby and in four time binnings, and the significance is evaluated once per sidereal day. Severe correlations exist in both space and time, although no simple distribution for an excess can be used to calculate the chance probability. In this case, a Monte Carlo simulation that emulates the search procedure, including the search for the maximum significance from 24 cell shifts and four time binnings, for a single source is constructed to sort the significance distribution, assuming that there are no signal emissions from the source. Fig. 6 presents the simulation results, with a mean value of 1.814, RMS of 0.705, and

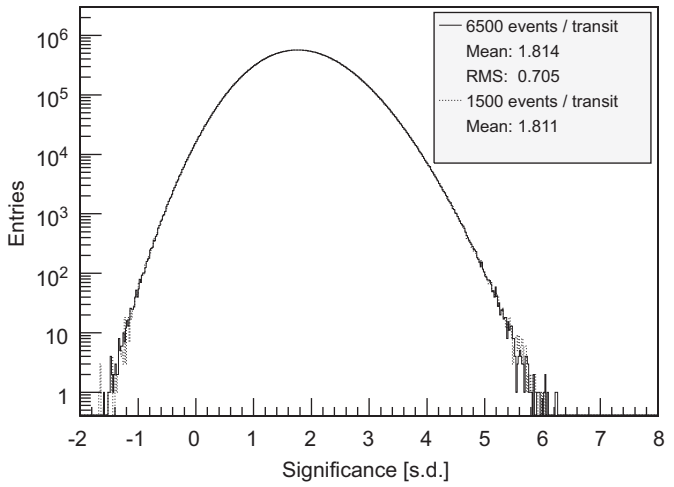

Fig. 6. Distribution of significances obtained from an MC simulation. Two samples with different background intensities are drawn in a superposition.

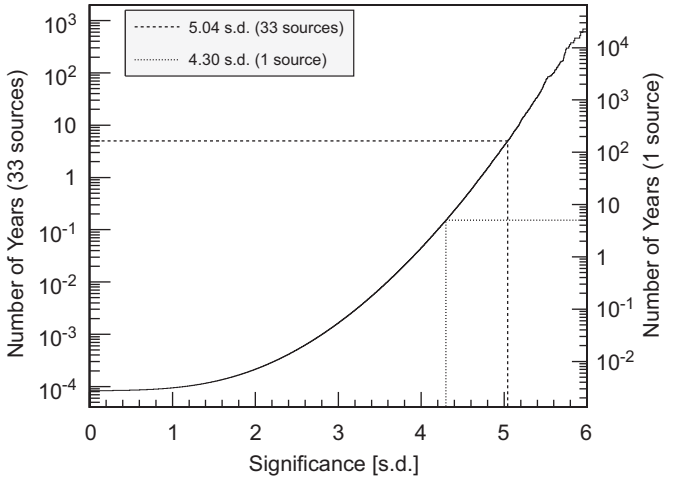

Fig. 7. Number of years for 1 occurrence against the significance threshold. The left *y*-axis corresponds to the 33 sources, whereas the right one represents a single source.

the number of entries corresponding to the number of days. Reasonably a Gaussian distribution is not followed. Further simulation revealed that this distribution did not depend on the background intensity in the sky cell, as shown by the two superposition curves in the plot.

From the plot, the chance probability for a significance threshold can be calculated easily. After converting the chance probability to time duration, the relationship between the number of years for a single source (or all 33 sources) and the significance threshold can be obtained (Fig. 7). Thresholds of 4.30 and 5.04 s.d. correspond to a chance probability of once per 5 years for a single source and all 33 sources, respectively. The chance probability of once per 5 years indicates that fake alarms brought by background fluctuations would happen once, at most, in the remaining duration of ARGO-YBJ.

The 33 sources are classified into two categories based on the observation history of ARGO-YBJ: (i) sources that have been observed, such as Mrk 421, and (ii) sources whose flares have not been detected yet. The threshold for sources in the first category is set to 4.30 s.d., and that for the other is 5.04 s.d. Once a source were detected to exceed its threshold, an alarm email would be immediately and automatically sent to the people concerned.

When a source in category (ii) is detected above its threshold, it would be manually elevated to category (i). This guarantees that the source would be monitored in a more active state hereafter, and any subsequent flares can be reported in a more timely manner.

In addition to the occasional alarm e-mail, daily reports summarizing excess information on all the sources for the past day are sent to the people concerned. This monitors the running status of the whole analysis procedure. In the future, all daily reports for all sources would be released on a public Web page, similar to what Fermi-LAT [12] and Swift [13] have done.

In summary, the monitoring chain is composed of raw data reconstruction, search for excess around selected sources, and alarm information release.

5. Results of the test run

The monitoring procedure described above has been preliminarily established in June 2010. A test to detect the past flares of Mrk 421 is undertaken using a total of 12 months data, including from January to June 2008 and from January to June 2010 when Mrk 421 was active. All the two flares of Mrk 421 (June 2008 and February 2010) detected by ARGO-YBJ are re-discovered and alarmed in 8-, and 4-day transits; a third Mrk 421 flare, occurred in March–April 2008, which is coincident with Swift data and was also observed by ARGO-YBJ with other methods (reported internally in the collaboration), is detected

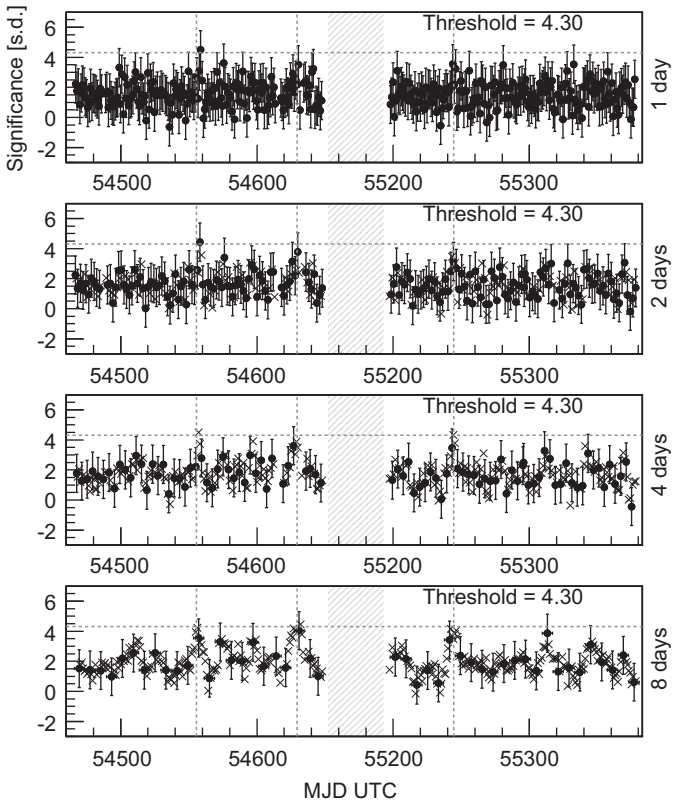

Fig. 8. Monitoring history of Mrk 421. The rolling significance around Mrk 421 for 1, 2, 4, and 8 transits can be seen. The significances and their errors are represented, respectively, by black dots and black error bars. The vertical dashed lined represents the peak time of flaring events from Swift, which were also observed by the ARGO-YBJ experiment. The two nonadjacent periods are linked by the gray shaded bands. For clarity, only exclusive data points are drawn with solid markers; others are drawn with cross-signs without error bars.

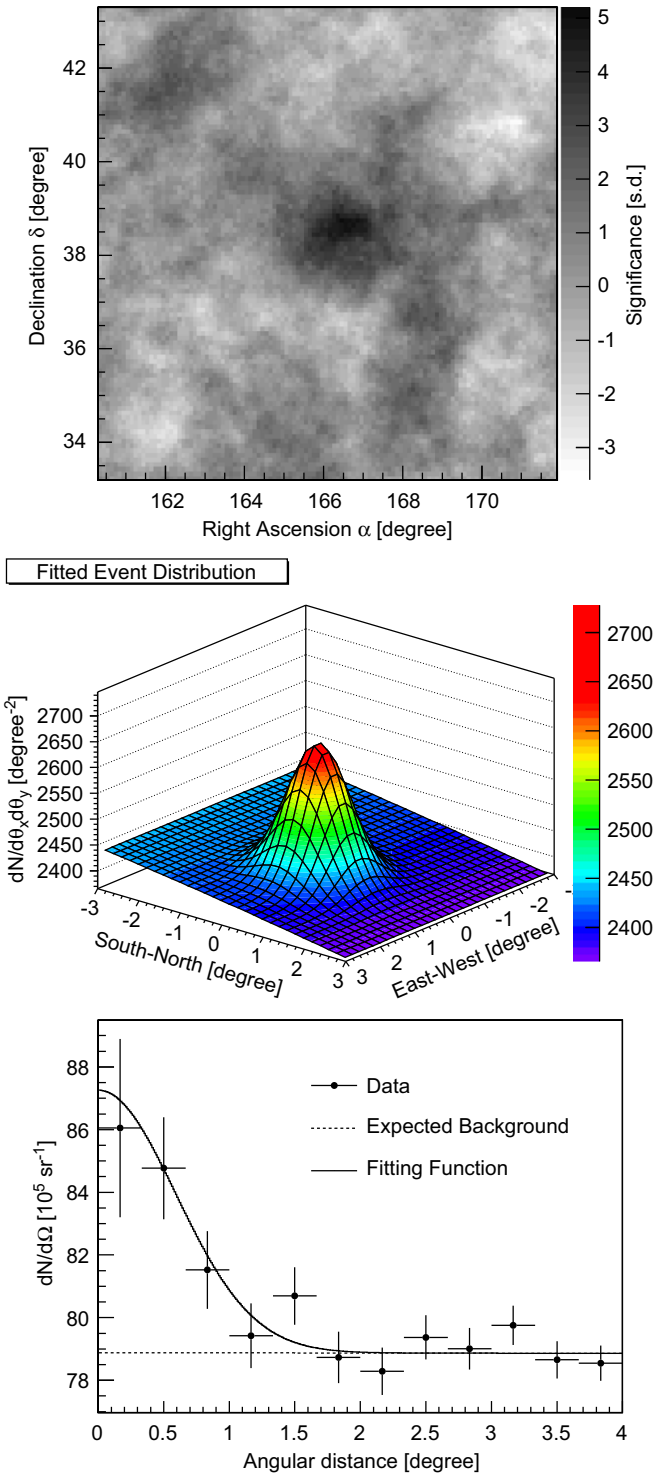

Fig. 9. Sample results of the follow-up analysis. Top: smoothed contour plot obtained by equi-zenith analysis; Middle: fitted event distribution; Bottom: projected radial distribution of events and the fitted function.

too in this analysis in 1-day transit; see Fig. 8 for the evolution of the significance, from which the three flares can be identified clearly. This proves the validity of the whole analysis scheme.

During the test run, once an alarm is produced, two further online checks are implemented assuming that the excess is due to a flaring of signal from a point source. First, the equi-zenith method [14] is used to cross-check and to obtain a significance contour plot of the excess. Second, a two-dimensional maximum-likelihood fit to the event distributions [7] is carried out. These follow-up analyses are completed in 3 h, and the results are sent by e-mail to the designated recipients. Fig. 9 shows a sample plot for the Mrk 421 flare from March 30 to April 2, 2008. From the fitted parameters, the following information about this excess can be obtained: (1) Position: $\Delta\alpha = 0.6 \pm 0.2^\circ$, $\Delta\delta = 0.3 \pm 0.2^\circ$, (2) Number of fitted excess events: 562 ± 145.

6. Summary

With the high duty cycle and wide field of view of the ARGO-YBJ detector, a real-time monitoring and alerting system for selected VHE extragalactic sources is established. Data of any candidate source can be analyzed within 3 h after it ends the transit in the local sky, and a detected flare event can be notified to the community soon after the analysis. The monitoring procedure has been successfully proven to be capable of detecting and reporting three Mrk 421 flares. A Web page to release daily monitoring reports is currently under construction.

Acknowledgement

This work is supported in China by NSFC (No. 10120130794), the Chinese Ministry of Science and Technology, the Chinese Academy of Science, the key Laboratory of Particle Astrophysics, CAS, and in Italy by the Istituto Nazionale di Fisica Nucleare (INFN).

The authors also acknowledge the support of W.Y. Chen, G. Yang, X.F. Yuan, C.Y. Zhao, R. Assiro, B. Biondo, S. Bricola, F. Budano, A. Corvaglia, B. D'Aquino, R. Esposito, A. Innocente, A. Mangano, E. Pastori, C. Pinto, E. Reali, F. Taurino and A. Zerbini, in the installation, debugging and maintenance of the detector.

References

[1] R. Wagner, ⟨http://www.mppmu.mpg.de/∼rwagner/sources/⟩.
[2] S. Wakely, D. Horan, ⟨http://tevcat.uchicago.edu/⟩.
[3] G. Aielli, et al., ARGO-YBJ Collaboration, Astrophysical Journal Letters 714 (2010) L208.
[4] B. Bartoli, et al., ARGO-YBJ Collaboration, Astrophysical Journal 734 (2011) 110.
[5] G. Aielli, et al., ARGO-YBJ Collaboration, Nuclear Instruments and Methods A 562 (2006) 92.
[6] A. Aloisio, et al., ARGO-YBJ Collaboration, IEEE Transactions on Nuclear Science NS-51 (2004) 1835.
[7] O. Adriani, et al., L3+C Collaboration, Astroparticle Physics 33 (2010) 24.
[8] F. Aharonian, et al., HEGRA Collaboration, Astrophysical Journal 614 (2004) 897.
[9] G. Aielli, et al., ARGO-YBJ Collaboration, Astroparticle Physics 30 (2009) 287.
[10] T.P. Li, Y.Q. Ma, Astrophysical Journal 272 (1983) 317.
[11] G. Aielli, et al., ARGO-YBJ Collaboration, Astrophysical Journal 729 (2011) 113.
[12] Fermi Collaboration, Multiwavelength Observations, ⟨http://fermi.gsfc.nasa.gov/science/multi⟩.
[13] Swift Collaboration, Swift/BAT Hard X-ray Transient Monitor, ⟨http://heasarc.gsfc.nasa.gov/docs/swift/results/transients⟩.
[14] M. Amenomori, et al., AS-Gamma Collaboration, Astrophysical Journal 633 (2005) 1005.